

Comparison of Analytical Calculations to Finite-Difference Time-Domain Simulations of One-Dimensional Spatially Varying Anisotropic Liquid Crystal Structures

Charles M. Titus^{1,*}, Philip J. Bos¹, Jack R. Kelly¹, and Eugene C. Gartland²

¹ Liquid Crystal Institute, Kent State University, Kent, OH, 44242, USA

² Department of Mathematics and Computer Science, Kent State University, Kent, OH, 44242, USA

* E-mail address: cmmt@columbo.kent.edu

(Received November 2, 1998; accepted for publication December 7, 1998)

There is a need for an accurate optical simulation tool for liquid crystal structures with director variations in more than one dimension. Finite-difference time-domain (FDTD) computation of Maxwell's equations is one approach to consider. The FDTD method has been in use in the electrical engineering community for years, but has only recently been applied to liquid crystal structures. Little is known about the accuracy of FDTD simulations of typical liquid crystal structures, in which the dielectric tensor can undergo large local spatial variations. This paper compares FDTD simulations and analytic solutions of two liquid crystal problems: the twisted-nematic cell and Bragg reflection from a planar cholesteric layer.

KEYWORDS: liquid-crystal, cholesteric, nematic, simulation, modeling, FDTD, optics

1. Introduction

The early years of liquid crystal display technology saw wide use of simple structures such as the twisted-nematic cell. Because of the use of relatively large pixels, the liquid crystal director (and thus the dielectric tensor) could be regarded as varying in only one dimension, normal to the display surfaces. Several methods, such as the extended Jones method¹⁾ and the Berreman matrix method²⁾, have been satisfactorily employed for optical analysis of these relatively simple liquid crystal displays. These methods are restricted to or designed specifically for simulations of one dimensional director structures

Recent advances in liquid crystal display technology make increasing use of pixels which can be smaller, contain multiple domains, or, as with in-plane switching, possess intentionally significant multidimensional spatial inhomogeneities of the liquid crystal director orientation. With these display technology advances there is an increasing need for a more sophisticated, multidimensional optical modeling tool. There have been some attempts to use the one-dimensional methods in these cases. One such technique involves dividing the structure into layers and columns. Each column is regarded as an independent one-dimensional structure. One of the one-dimensional methods is then applied to each column. However, such adaptation of one-dimensional techniques to two-dimensional problems cannot properly take into account lateral scattering of light propagating within the liquid crystal structure. Nor can those methods accurately calculate the propagation of obliquely incident light through a liquid crystal structure with director variations in more than one dimension.

There are other interesting liquid crystal devices for which optical simulation requires making assumptions and simplifications which may impact the accuracy of the simulation. There has been some interest in the use of liquid crystal phase gratings for beam steering applications^{3,4)}. In those devices, the phase profile is achieved by applying a distribution of voltages to an array of separated electrodes on the surface of a liquid crystal film. Optical simulations of such structures have been conducted which assume simplified liquid crystal director configurations. In those analyses, it is assumed that the liquid crystal director varies only in the direction parallel to the grating surface, ignoring the effect of fringing fields.

For these and other reasons, the Finite-difference time-domain (FDTD) computation of Maxwell's equations has recently been considered for use as an optical simulation tool for liquid crystal structures

with generally inhomogeneous director orientation⁵). FDTD, as introduced by Yee⁶ for isotropic media, makes use of direct discretization of the general form of Maxwell's equations. Because of this, the FDTD method can accommodate multidimensional inhomogeneity of the dielectric tensor.

However, it must not be forgotten that the FDTD method provides a numerical *approximation* of the solution to Maxwell's equations. The accuracy this method has been tested for a variety of structures and media, including some anisotropic media⁷. None of these tests, however, cover the inhomogeneous dielectric anisotropy characteristic of advanced liquid crystal displays. In particular, liquid crystal structures can contain defects, such as disclinations, which result in large variations of the dielectric tensor over sub-wavelength distances. Some analysis is necessary in order to know how to apply FDTD modeling to liquid crystal structures in cases ranging from slowly varying director orientation found in in-plane switching to structures containing defects.

Toward that end, we present here a comparison of FDTD and analytic solutions for several well-known liquid crystal problems. The first such case is the transmission of light through a twisted-nematic cell, following the analysis of Gooch⁸. The second and third cases cover Bragg reflection from a planar cholesteric layer for low and high birefringence materials⁹. These examples will quantify the problems which become more pronounced with increasing rate of spatial variations of the anisotropic dielectric tensor found in the vicinity of the defect cores. These are only one-dimensional problems, but it is hoped that observations made here may assist in proper application of the FDTD method in order to accurately model multidimensional liquid crystal problems.

2. Background

At the heart of the FDTD method is the spatial discretization of the structure to be analyzed, and the use of central finite differences to approximate Maxwell's equations. An oscillating wave source is introduced into the grid and the entire grid is time-stepped until steady state oscillations are obtained at all points on the grid. The previous FDTD simulation of liquid crystals employs this technique, modified for sourceless inhomogeneous anisotropic media⁵):

$$\frac{\partial E(r)}{\partial t} = \varepsilon^{-1}(r) \cdot [\nabla \times H(r)] \quad (1)$$

$$-\frac{\partial H(r)}{\partial t} = \mu_0^{-1} \cdot [\nabla \times E(r)] \quad (2)$$

where $\varepsilon^{-1}(r)$ is the inverse of the spatially varying dielectric tensor. This paper uses the same technique. After discretization in time employing the central finite difference, eqs. (1) and (2) can be used as follows to update the three vector components of both fields:

$$E_i |^{n+1} = E_i |^{n+1/2} + \Delta t \cdot \varepsilon_{ij}^{-1}(r) \cdot \varepsilon_{jkl} \cdot \frac{\partial}{\partial x_k} H_l |^{n+1/2} \quad (3)$$

$$H_i |^{n+1/2} = H_i |^{n-1/2} - \frac{\Delta t}{\mu_0} \cdot \varepsilon_{ijk} \cdot \frac{\partial}{\partial x_j} E_k |^n \quad (4)$$

where subscripts $i,j,k,l=(x,y,z)$ indicate rectilinear coordinate axes, and summation convention is used. The symbol ε_{ijk} represents the Levi-Civita permutation symbol. The i,j component of the inverted dielectric tensor at any grid location r is denoted $\varepsilon_{ij}^{-1}(r)$. The superscript n denotes the discrete time coordinate, and Δt is the time step resulting from finite difference approximation of the time derivative. Spatial derivatives above are not discretized for the sake of simplicity, but they, too, are approximated with central finite differences. For example, in a one-dimensional problem whose grid is the z -axis, the partial derivatives with respect to x and y do not exist. In that case, full discretization of the x -component of eq. (3) would yield:

$$E_x |_K^{n+1} = E_x |_K^n + \frac{\Delta t \cdot \varepsilon_{xx}^{-1} |_k}{\Delta h} [H_y |_{K-1/2}^{n+1/2} - H_y |_{K+1/2}^{n+1/2}] + \frac{\Delta t \cdot \varepsilon_{xy}^{-1} |_k}{\Delta h} [H_x |_{K+1/2}^{n+1/2} - H_x |_{K-1/2}^{n+1/2}] \quad (5)$$

where Δh is the separation of the two grid nodes surrounding the location at which E is being updated. The first subscript in field terms indicates vector component and the second subscript denotes location on the grid. Similarly, the first subscript in the inverted dielectric tensor denotes the tensor component and the second denotes the grid location at which it is evaluated.

The previous liquid crystal study employed the second-order Mur treatment¹⁰⁾ for terminating the grid. Testing of the Mur absorbing boundary revealed that it was not as efficient as required for the following analysis. Reflections of waves incident upon the Mur boundary were, over many time steps, of sufficient magnitude to influence FDTD results. For this reason, the more effective “Perfectly matched layer” (PML) absorbing layer¹¹⁾ was used for the simulations in this study.

The Mur grid termination technique applies a numerical solution to the wave equation along the grid boundary. It is computationally less expensive and easier to implement than the PML. The PML is implemented as an absorbing layer which surrounds the inner computational domain. It consists of a fictitious lossy medium which incorporates magnetic as well as electric conductivity:

$$\epsilon \frac{\partial E}{\partial t} + \sigma E = \nabla \times H \quad (6)$$

$$- \mu \frac{\partial H}{\partial t} - \sigma^* H = \nabla \times E \quad (7)$$

Impedance matching of the PML with the adjacent inner computational domain makes that interface very transmissive to waves radiating from the inner grid. As a result, most of the radiation reaching the boundary passes into the PML and decays rapidly.

The difference between the two treatments can be seen in a simple test. An oscillating point source is placed asymmetrically in a square grid. The source and grid are time-stepped, allowing emitted waves to propagate out to the boundary until reflections from the grid boundaries, if they exist, return to the location of the point source. Since the source is asymmetrically placed in the grid, any reflections which occur will show up as an asymmetry of the field around the source. This test was conducted for the Mur and PML treatments. The resulting field magnitudes at grid locations in the neighborhood of the point source are shown in Tables I and II. Use of the Mur boundary (Table I) resulted in significant asymmetry,

indicating the presence of boundary reflections. No such asymmetry was seen when the PML was employed (Table II).

Illumination of liquid crystal structures in this study was provided by means of the separate-field formulation¹²⁾. In this technique, the inner computational domain is divided into two regions. In the inner region the total field, the superposition of the source and the scattered fields is calculated. In the outer region, only the scattered field is calculated. The source is introduced at the interface between these two regions, added into Maxwell's equations on the inner side of the interface and subtracted on the outer side. Unlike other means of illumination, such as the soft source¹³⁾, this technique can produce diffraction-free plane waves in simulations for which periodic boundaries are not appropriate. That is not important for the one-dimensional simulations below, but does permit extension of this work to aperiodic liquid crystal structures.

2.1 Stability

Limiting the size of the time step is necessary in order to prevent growth of numerically induced oscillations. The limit for a one-dimensional FDTD grid is expressed in the following relation¹³⁾:

$$\Delta t \leq \frac{\Delta h}{v_{\max}} \quad (8)$$

where Δt is the size of the time step and v_{\max} is the maximum phase velocity of waves traveling on the grid. The spatial step Δh is the size of the standard Yee cell (two node separations across), normally defined as λ/N , where N is some integer. For an isotropic spatially varying dielectric, $v = v(r) = c/n(r)$. The maximum phase velocity then occurs for the minimum refractive index on the grid, so:

$$\Delta t \leq \frac{\Delta h \cdot n_{\min}}{c} \quad (9)$$

This was used as a stability guideline for spatially varying anisotropic media in the simulations below.

2.2 Accuracy

Since the subject of this study is the accuracy of FDTD simulations of liquid crystal structures, some discussion of factors contributing to FDTD inaccuracy is useful. FDTD inaccuracies result from the temporal and spatial discretization of the problem. For instance, the second-order accurate central finite difference approximations used in this study are somewhat less than exact.

Such discretization can manifest itself in numerical dispersion¹²⁾, which is the departure of numerical phase velocity from that which would occur in continuous space. In particular, the phase velocity of waves in an FDTD simulation is always less than the continuous-space value. In other words, as will be shown below, the numerical wavelength is always less than the continuous-space value. The numerical dispersion relation for a spatially varying anisotropic dielectric is not trivial. A clearer picture of grid-induced dispersion for that case can be drawn from a similar relation for isotropic media. The numerical dispersion relation is derived by substitution of a trial plane wave solution into the discretized Maxwell's equations¹²⁾. For a uniformly discretized grid, the plane wave is given the form:

$$E_{L,I,J,K}^n = E_{L0} e^{i(k_x I \Delta h + k_y J \Delta h + k_z K \Delta h - \omega n \Delta t)} \quad (10)$$

$$H_{L,I,J,K}^n = H_{L0} e^{i(k_x I \Delta h + k_y J \Delta h + k_z K \Delta h - \omega n \Delta t)} \quad (11)$$

where L denotes the field's vector component, (I,J,K) indicate position on the grid, and n is the current time step. The angular frequency of the wave is ω and wavevector components are k_x , k_y , and k_z . This plane wave is substituted into the system of discretized update equations for an isotropic medium, similar to the form seen in eq. (5). The numerical dispersion relation results from elimination of the field magnitudes E_{L0} and H_{L0} from the system of equations. The result can be simplified for the one-dimensional case:

$$\frac{1}{v^2 \Delta t^2} \sin^2 \left(\frac{\omega \Delta t}{2} \right) = \frac{1}{\Delta h^2} \sin^2 \left(\frac{k_n \Delta h}{2} \right) \quad (12)$$

where v is the continuous-space phase velocity, ω is the frequency of the propagating radiation, and k_n is the effective numerical wavenumber resulting from the discretization of the problem. Introducing into this equation spatial variation of the isotropic dielectric constant through $v = c/n(r)$, defining the spatial step size $\Delta h = \lambda_{\min}/N = \lambda_0/(N \times n_{\max})$, with $\omega = ck_0 = 2\pi c/\lambda_0$, and utilizing the limiting value of eq. (9), then eq. (12) becomes:

$$\lambda_n(r) = \lambda_c(r) \cdot \frac{n(r)}{n_{\min}} \cdot \frac{\pi}{N \cdot \sin^{-1} \left(\frac{n(r) \cdot n_{\max}}{(n_{\min})^2} \sin \left(\frac{\delta \cdot n_{\min}}{N \cdot n_{\max}} \right) \right)} \quad (13)$$

$$\lambda_c(r) = \frac{\lambda_0}{n(r)} \geq \lambda_n(r) \quad (14)$$

where λ_c is the continuous-space value of the wavelength and λ_n is the numerical value caused by discretization. From eq. (13), it appears that waves propagating within the grid have a shorter length than the continuous-space value. Spectral data generated by FDTD simulations will thus be shifted to longer wavelengths. As the grid is refined (increasing N), this shift is reduced. If the refractive index profile $n(r)$ is known for this spatially varying isotropic dielectric, it may be possible to calculate the amount of shift. However, for spatially varying anisotropic dielectrics that task is difficult.

The magnitude of this shift depends on spacing between nodes on the grid, time step size, dielectric properties, and the frequency of the propagating wave, as can be seen in the numerical dispersion relation eq. (12). Because time-stepping to a steady-state FDTD result may require accounting for multiple reflections, the impact of numerical dispersion also depends on the size of the structure to be analyzed and the number of time steps required to reach steady state.

Of these factors, only the time step size and node spacing are not predetermined by the problem at hand. One might expect that as time step and node spacing approach zero, errors are reduced and the FDTD result approaches the exact solution. This behavior for node spacing is confirmed in the results below. However, as has been found in previous studies^{14,15}, FDTD results are more accurate when the time

step is equal to, not less than, its maximum stable value. This may be due in part to the fact that as the time step is decreased, more steps are necessary to reach steady state, increasing the impact of roundoff error¹⁵⁾,

In addition, the continuous spatial variations of the dielectric tensor of liquid crystal structures are discretized. This may lead to field discontinuities and spurious reflections which are numerical in origin and not at all representative of actual light propagation through such structures. We have not yet determined if this is a significant source of error. If such error does occur, it will decrease as the node spacing is decreased.

Thus, the only control over accuracy at our disposal is the choice of node spacing. The case studies below investigate the impact of node spacing on accuracy of FDTD simulations of some liquid crystal structures.

3. Experimental

For all the simulations below, a $6\Delta h$ (12 nodes) thick PML was employed. The conductivity was given a cubic profile:

$$\sigma(r) = \sigma_{\max} \left(\frac{r}{d} \right)^3 \quad (15)$$

where r is the distance into the PML, measured normal to the interface with the inner computational domain, d is the PML thickness, and $\sigma_{\max} = 5 \times 10^7 \text{ } \Omega^{-1} \text{m}^{-1}$. This is the same PML implementation as was used in the above comparison with the Mur boundary treatment. No attempt was made to optimize the PML.

In all cases, the magnitude of the time step was determined from the limit in eq. (9). For example, the low-birefringence cholesteric below has ordinary and extraordinary refractive indices of 1.465 and 1.535, respectively. The liquid crystal was embedded in glass, $n = 1.5$. For $\lambda = 0.5 \mu\text{m}$ and $\Delta h = \lambda/20$, $\Delta t = 1.22 \times 10^{-16}$ s.

The source employed in each of the simulations was a plane wave, propagating along the one-dimensional grid (z -axis), of form:

$$E(z, t) = \text{Re}\{E_0 e^{i(kz - \omega t)}\} \quad (16)$$

where $k = 2\pi/(\lambda_0 n)$ for a source implemented in glass ($n=1.5$) in all cases below, z is the position on the grid, $\omega=ck_0$, and t is the elapsed time. In all cases, the magnitude $E_0 = 1$. The vector E_0 dictates the polarization of the source. The source for twisted-nematic simulations was linearly polarized source, and for the planar cholesteric simulations it was circularly polarized with the same rotation sense as the cholesteric helix.

4. Results

The three cases below follow a progression which is intentional. The liquid crystal medium in each case exhibits greater spatial variation of anisotropic dielectric properties than its preceding case. As was mentioned earlier, this is designed to cover the range of variations which might occur within real liquid crystal simulations. Spatial variation of the dielectric tensor can be accomplished by one of three means: increasing the spatial rate of change of the liquid crystal director, increasing the material's birefringence, or a combination of the two.

4.1 Case I: The twisted-nematic cell

The previous application of FDTD to liquid crystal simulations presented a qualitative illustration of FDTD-computed polarization rotation by a twisted-nematic (TN) cell⁵⁾. What follows is a quantitative comparison of FDTD simulations of a TN cell with the exact analytical results. The twisted-nematic liquid crystal problem is characterized by relatively small spatial variations of the dielectric tensor. Nevertheless, analysis shows that some attention to the node spacing is required to produce quantitatively accurate numerical results.

The test cell placed in the FDTD grid consisted of a 5 μ m-thick 90° TN layer. The liquid crystal was given an ordinary refractive index $n_o=1.5$ and a variable extraordinary index n_e . The layer was placed inside an isotropic medium with a refractive index $n=1.5$ (i.e. common glass). The cell was illuminated by a source linearly polarized perpendicular to the liquid crystal director at the entry surface. An optional ideal polarizer was aligned perpendicular to the liquid crystal director at the exit interface between liquid crystal and glass. Reflected and transmitted intensities were measured inside the glass. All results were normalized to the source intensity in the glass. For this orientation of liquid crystal and incident light

polarization, maintaining the liquid crystal's ordinary index at 1.5 eliminated reflections at the entry interface between liquid crystal and glass.

Earlier work by Gooch⁸⁾ provided an analytical expression for intensity transmitted through a similar undisturbed twisted-nematic layer as a function of $\Delta nd/\lambda$. That analytical calculation is the benchmark for comparison with FDTD results.

FDTD computations of the above structure were conducted with node spacings of $\lambda/20$ and $\lambda/40$. Steady state was obtained nearly as quickly as for an isotropic slab of the same thickness (Fig. 1). As expected, cutting the node spacing in half doubled the number of time steps necessary to reach steady state (because Δt is proportional to Δh). The FDTD results showed the same qualitative behavior as the Gooch curve (Fig. 2), with only a small numerical error. The FDTD results appeared to be shifted to longer wavelengths, which is characteristic of numerical dispersion.

The error contained in the numerical results was illustrated differently in Fig. 3, which displays the absolute difference between FDTD and analytical results as a function of $\Delta nd/\lambda$. For a node spacing of $\lambda/20$, the numerical error may be unacceptable for some analyses. Reducing the node spacing by one-half, to $\lambda/40$, reduced the error to one-fourth that which occurs for a node spacing of $\lambda/20$. In general, one can expect such reduction because the central finite difference formula employed here is "second-order accurate" in both time and space.

4.2 Case II: Bragg reflection from a low-birefringence cholesteric

Uniform cholesteric liquid crystal layers are known to exhibit Bragg reflection of wavelengths comparable to the cholesteric pitch. An exact analytical solution for this problem can be found in ref. 9.

The cholesteric structure here was designed to provide moderately larger spatial variations of the dielectric tensor than in the twisted-nematic cell above. The test cell consisted of a planar cholesteric layer $6\mu\text{m}$ thick, with a pitch of $0.3333\mu\text{m}$. The cholesteric helix was oriented normal to the interface between glass and liquid crystal. The ordinary and extraordinary refractive indices of the cholesteric liquid crystal were 1.465 and 1.535, respectively. The cell was again placed between glass ($n=1.5$) substrates. Illumination was provided by circularly polarized light at normal incidence, with a rotation sense matching that of the liquid crystal helix. Reflected and transmitted intensities were again measured inside the glass

to avoid the effects of the air-glass interface. Normalizing the reflected and transmitted intensities to the source intensity in the glass provided optical reflectivity (R) and transmissivity (T) of the cholesteric layer.

Steady state solution (Fig. 4) required many more time steps than for the twisted-nematic layer of similar thickness. This may be strictly the result of Bragg reflections working their way through the simulation. For a node spacing of $\lambda/20$, the FDTD-computed reflectivity spectrum is clearly inaccurate (Fig. 5). Numerical dispersion, evidenced by the shift of numerical results to longer wavelengths, is apparent for the coarser grid. Substantially reduced deviation between analytical and numerical reflectivity required a node spacing of $\lambda/50$, finer than required for the twisted-nematic problem.

It is interesting to note that energy was not conserved for the coarser grid (Fig. 6). In particular, there were problems outside the main Bragg reflection band, more significant at the steeper portions of the reflection spectrum. At those wavelengths, the coarse-grid FDTD results may be more sensitive to another numerical problem such as cancellation error. The finer grid displayed no such problem.

4.3 Case III: Bragg reflection from a high-birefringence cholesteric

The final comparison involved a test cell identical to the above cholesteric problem, except that the liquid crystal birefringence has been increased ($n_e=1.7$, $n_o=1.5$). This case was chosen to provide larger spatial variation of dielectric tensor than the first cholesteric cell above. In this case, the dielectric variations are similar to those near a liquid crystal defect.

Steady state required many more time steps than for the low-birefringence cholesteric layer (Fig. 7), more than would be expected from the increased optical density. This may again be strictly rooted in the nature of the Bragg reflection, or it may be a numerical effect resulting from increased discontinuity of dielectric properties.

In this example, a node spacing of $\lambda/60$ was required in order to obtain substantial reduction of deviation between analytical and numerical reflectivity (Fig. 8). This is a finer grid than required for the low-birefringence cholesteric case. The trend is obvious. As the spatial variations of the dielectric tensor increase, finer gridding is required in order to obtain accurate results from FDTD simulation.

The energy conservation problems observed in the coarse-grid simulation of the low-birefringence cholesteric were again apparent for the coarse grid here (Fig. 9).

5. Discussion

Without resorting to higher-order finite-differences or other means of removing numerical dispersion, choice of node spacing is the only simple means of achieving accurate FDTD results for liquid crystal structures.

As the twisted-nematic case above has illustrated, accurate FDTD results can be obtained at moderate node spacing for liquid crystal problems with slowly varying dielectric tensor. It is reasonable to expect that the FDTD method can accurately simulate liquid crystal problems without defects.

As spatial variation of the dielectric tensor increases, finer node spacing is required in order to obtain accurate FDTD computation. Note that it is not the spatial rate of change of the liquid crystal director that is important. Maxwell's equations do not explicitly consider the orientation of molecules. Rather, it is the spatial rate of change of the dielectric tensor, which is influenced by both the molecular orientation and the molecular dielectric anisotropy. The most severe of the three cases above exhibits spatial variations of dielectric tensor similar to those seen in disclinations. Accurate FDTD simulations of liquid crystal structures containing significant defects may require a very fine grid, perhaps as small as $\lambda/60$. How fine the grid should be will depend on the significance of defects in the liquid crystal structure being modeled. Of course, as node spacing is reduced for a fixed geometry FDTD problem, memory requirements increase and more time steps are required to reach steady state. For instance, if the node spacing is cut in half, the problem must be represented by twice as many nodes. And since the maximum stable time step size is proportional to node spacing, cutting the node spacing in half also necessitates twice as many time steps to reach a steady state solution. In general, computational expense increases roughly as the square of the relative increase of number of nodes per wavelength.

One solution may be to employ higher order finite-differencing techniques. Greater accuracy provided by such techniques may permit accurate FDTD computation on a coarser grid. But first, the savings of a coarser grid must be weighed against the increased computational cost of evaluating higher order finite differences. In addition, higher order finite-differencing may increase the difficulty of approximating Maxwell's equations across field discontinuities.

Another potential means of removing numerical dispersion is to add a corrective factor to the finite difference formula. The corrective factor accounts for the difference between numerical and continuous-space phase velocities. Such a correction is derived from the numerical and continuous-space dispersion relations. This has been accomplished for isotropic dielectrics¹²⁾, but not yet for spatially varying anisotropic media.

6. Conclusion

We have compared FDTD simulations and analytic solutions of two liquid crystal problems, the twisted-nematic cell and Bragg reflection from a planar cholesteric layer. Analysis suggests that attention must be paid to the magnitude of spatial variations of the dielectric tensor in order to obtain accurate FDTD simulations of liquid crystal structures. The analysis above is limited to one-dimensional problems, but nevertheless provides insight into the demands of FDTD simulations of liquid crystals.

Acknowledgements

The authors wish to express appreciation to the BMDO/AFSOR for funding this project, under grant #F49620-96-1-04494. Additional funding was supplied by ALCOM, under grant #DMR-8920147. Dr. Gartland was funded by the NSF, under grant #DMS-9870420. In addition, we thank Dr. Sergij Shiyankovskii and Dr. Oleg Lavrentovich for useful discussions.

- A. Lien: Appl. Phys. Lett.: **57** (1990) 2767.
1. D. W. Berreman: J. Opt. Soc. Am. **63** (1973) 1374.
 2. R. M. Matic: Proc. SPIE **2120** (1994) 194.
 3. P. F. McManamon, T. A. Dorschner, D. L. Corkum, L. J. Friedman, D. S. Hobbs, M. Holz, S. Lieberman, H. Q. Nguyen, D. P. Resler, R. C. Sharp, E. A. Watson: Proc. IEE **84** (1996) 268.
 4. B. Witzigmann, P. Regli, and W. Fichtner: J. Opt. Soc. Am. A **15** (1998) 753.
 5. K. S. Yee: IEEE Trans. Antenna. & Propag. **14** (1966) 302.
 6. J. Schneider, S. Hudson: IEEE Trans. Antenna. & Propag. **14** (1993) 994.
 7. C. H. Gooch, H. A. Tarry: J. Phys. D **8** (1975) 1575.
 8. H. Wohler, G. Haas, M. Fritsch, D. A. Mlynski: J. Opt. Soc. Am. A **5** (1988) 1554.
 9. G. Mur: IEEE Trans. Electr. Compat. **23** (1981) 377.
 10. J-P. Berenger: J. Comput. Phys. **114** (1994) 185.
 11. A. Taflove: *Computational Electrodynamics, The Finite-Difference Time-Domain Method* (Artech House, Boston, 1995).
 12. A. Taflove, M. E. Brodwin: IEEE Trans. Microwave Theory & Techniques **23** (1975) 623.
 13. I. S. Kim, W. J. R. Hofer: 1989 IEEE AP-S Symp. Dig. (1989) p.1108.
 14. I. S. Kim, W. J. R. Hofer: Electron. Lett. **26** (1990) 485.

TABLE 1: Second-order Mur boundary test. Electric field magnitudes surrounding hard point source (enclosed in box), located at node (21,31) within 100 X 100 free-space FDTD grid, $\lambda=0.5\text{mm}$, Δt at stability limit, $\Delta h=\lambda/40$, after 528 time steps. Employed first-order Mur boundary at corners.

0.032	0.051	0.063	0.066	0.060	0.045	0.024
0.081	0.108	0.126	0.131	0.124	0.105	0.078
0.134	0.170	0.197	0.207	0.196	0.170	0.135
0.189	0.239	0.279	0.296	0.279	0.241	0.193
0.243	0.312	0.376	0.413	0.377	0.315	0.248
0.289	0.382	0.490	0.592	0.492	0.385	0.294
0.314	0.426	0.599	0.959	0.601	0.429	0.319
0.306	0.399	0.507	0.609	0.508	0.401	0.310
0.277	0.345	0.409	0.446	0.409	0.346	0.279
0.239	0.288	0.328	0.345	0.327	0.288	0.238
0.198	0.234	0.260	0.269	0.259	0.232	0.195
0.157	0.184	0.202	0.208	0.200	0.180	0.151
0.117	0.138	0.151	0.154	0.148	0.132	0.109

Table I
 C. M. Titus, P. J. Bos, J. R. Kelly, E. C. Gartland
 Breadth: One column, 8.5 cm.

TABLE 2: PML boundary test. Electric field magnitudes surrounding hard point source (enclosed in box), located at node (21,31) within 100 X 100 free-space FDTD grid, $\lambda=0.5\text{mm}$, Δt at stability limit, $\Delta h=\lambda/40$, after 528 time steps. Pml is $6\Delta h$ thick (12 nodes), cubic conductivity profile.

0.153	0.174	0.188	0.193	0.188	0.174	0.153
0.202	0.228	0.246	0.253	0.246	0.228	0.202
0.251	0.286	0.310	0.320	0.310	0.286	0.251
0.301	0.346	0.382	0.397	0.382	0.346	0.301
0.346	0.408	0.464	0.496	0.464	0.408	0.346
0.382	0.464	0.559	0.647	0.559	0.464	0.382
0.397	0.496	0.647	0.959	0.647	0.496	0.397
0.382	0.464	0.559	0.647	0.559	0.464	0.382
0.346	0.408	0.464	0.496	0.464	0.408	0.346
0.301	0.346	0.382	0.397	0.382	0.346	0.301
0.251	0.286	0.310	0.320	0.310	0.286	0.251
0.202	0.228	0.246	0.253	0.246	0.228	0.202
0.152	0.174	0.188	0.193	0.188	0.174	0.153

Table I
 C. M. Titus, P. J. Bos, J. R. Kelly, E. C. Gartland
 Breadth: One column, 8.5 cm.

Figure Captions

FIG. 1: Number of time steps required to reach steady state FDTD results, twisted-nematic liquid crystal cell without polarizers. Results from two values of grid node separation, $\lambda/20$ and $\lambda/40$.

FIG. 2: Transmissivity through twisted-nematic cell with exit polarizer. Comparison of analytical curve to FDTD simulation results, $\lambda/20$ and $\lambda/40$.

FIG. 3: Difference between transmissivities obtained from analytical and FDTD computation of twisted-nematic cell, $\lambda/20$ and $\lambda/40$.

FIG. 4: Number of time steps required to reach steady state FDTD results, low-birefringence planar cholesteric layer. Results from two values of grid node separation, $\lambda/20$ and $\lambda/40$.

FIG. 5: Transmissivity through low-birefringence planar cholesteric layer. Comparison of analytical curve to FDTD simulation results, $\lambda/20$ and $\lambda/50$.

FIG. 6: Energy conservation (reflectivity plus transmissivity) of FDTD results for low-birefringence planar cholesteric layer, $\lambda/20$ and $\lambda/50$.

FIG. 7: Number of time steps required to reach steady state FDTD results, high-birefringence planar cholesteric layer. Results from two values of grid node separation, $\lambda/20$ and $\lambda/40$.

FIG. 8: Transmissivity through high-birefringence planar cholesteric layer. Comparison of analytical curve to FDTD simulation results, $\lambda/20$ and $\lambda/60$.

FIG. 9: Energy conservation (reflectivity plus transmissivity) of FDTD results for high-birefringence planar cholesteric layer, $\lambda/20$ and $\lambda/60$.

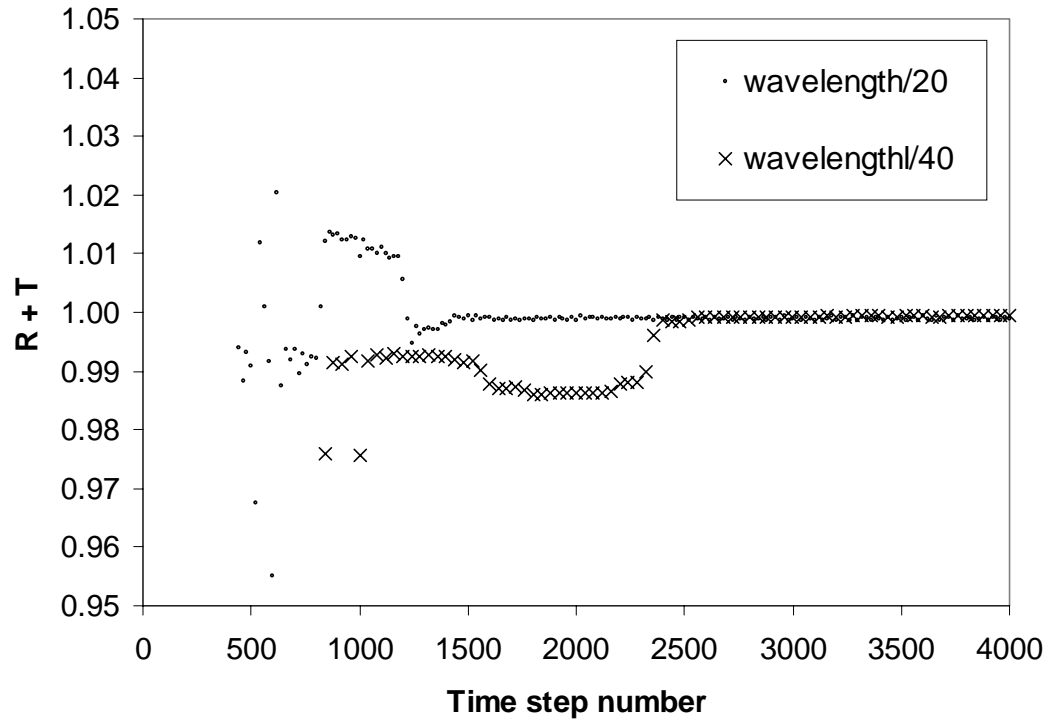


Figure 1
C. M. Titus, P. J. Bos, J. R. Kelly, E. C. Gartland
Breadth: One column, 8.5 cm.

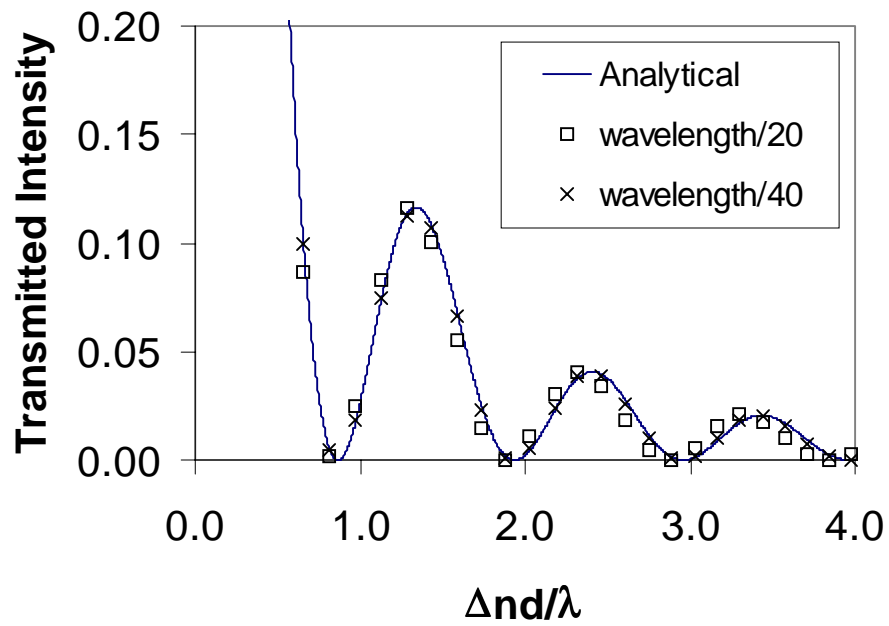


Figure 2
C. M. Titus, P. J. Bos, J. R. Kelly, E. C. Gartland
Breadth: One column, 8.5 cm.

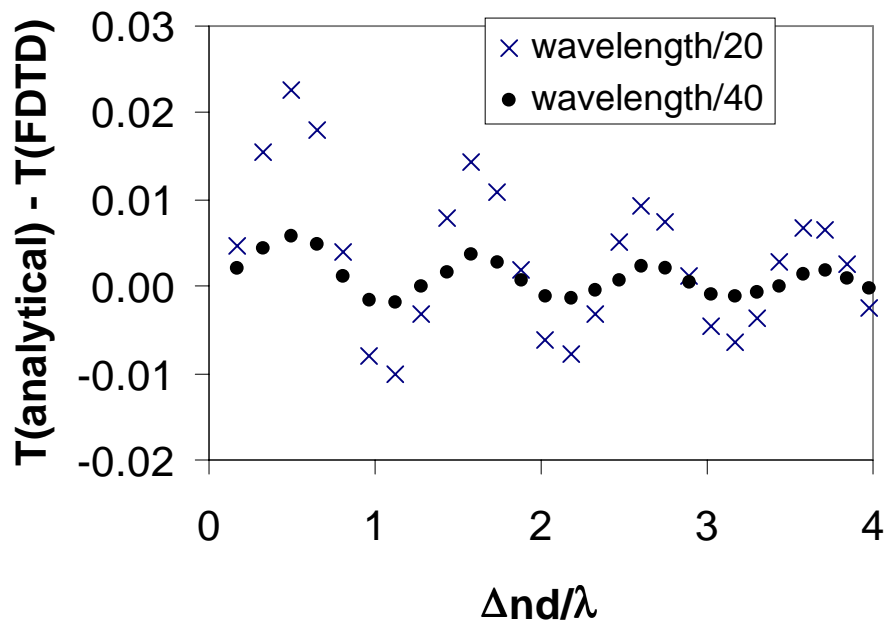


Figure 3
 C. M. Titus, P. J. Bos, J. R. Kelly, E. C. Gartland
 Breadth: One column, 8.5 cm.

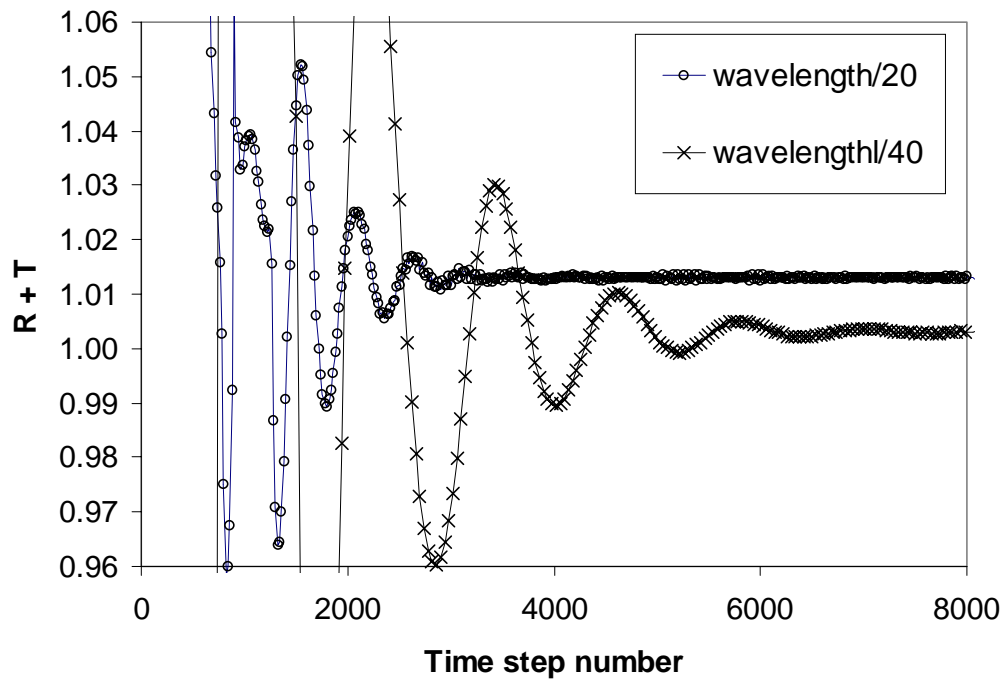


Figure 4
C. M. Titus, P. J. Bos, J. R. Kelly, E. C. Gartland
Breadth: One column, 8.5 cm.

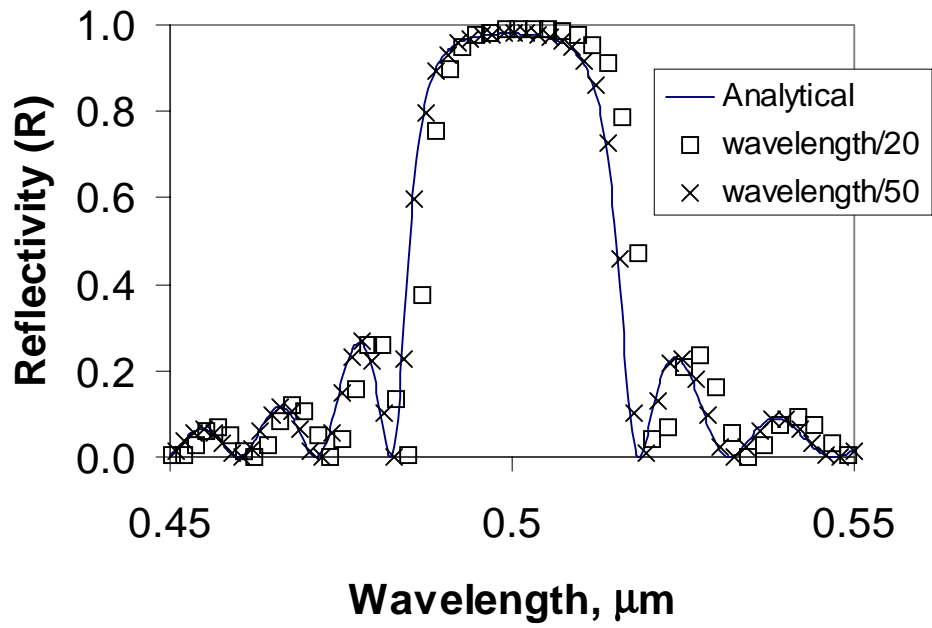


Figure 5
C. M. Titus, P. J. Bos, J. R. Kelly, E. C. Gartland
Breadth: One column, 8.5 cm.

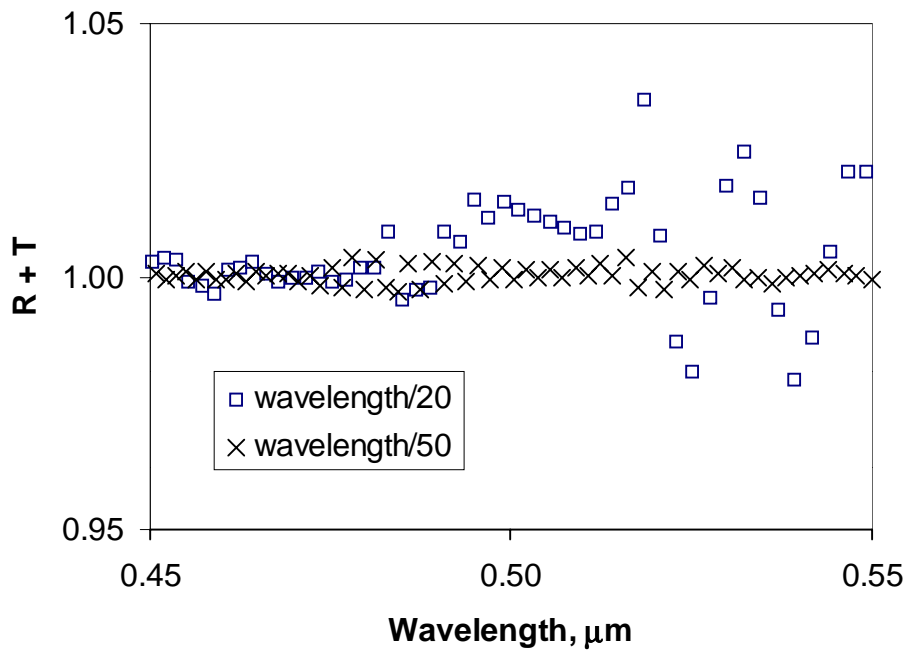


Figure 6
C. M. Titus, P. J. Bos, J. R. Kelly, E. C. Gartland
Breadth: One column, 8.5 cm.

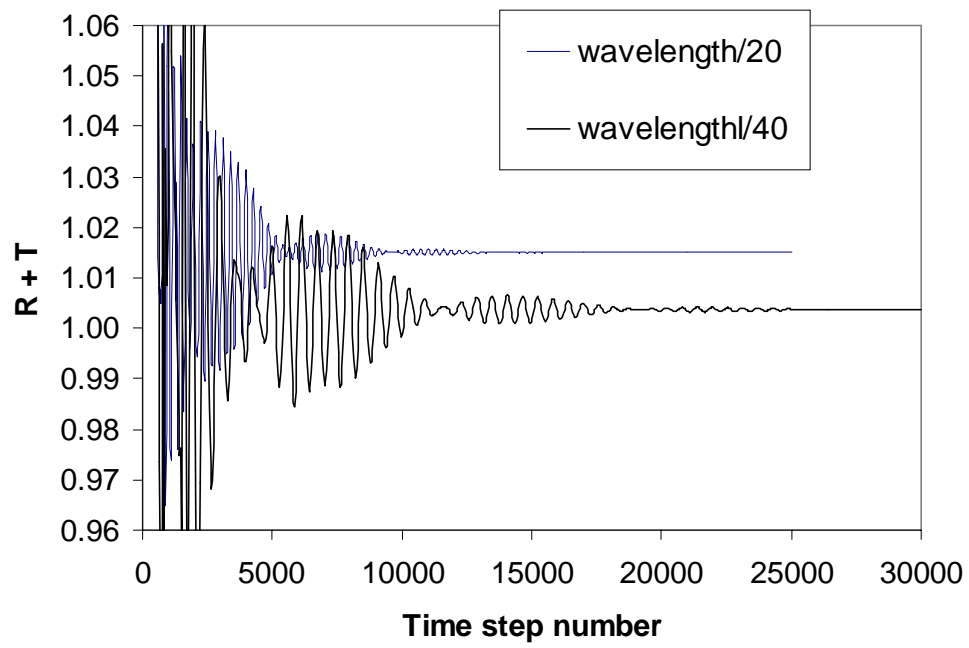


Figure 7
C. M. Titus, P. J. Bos, J. R. Kelly, E. C. Gartland
Breadth: One column, 8.5 cm.

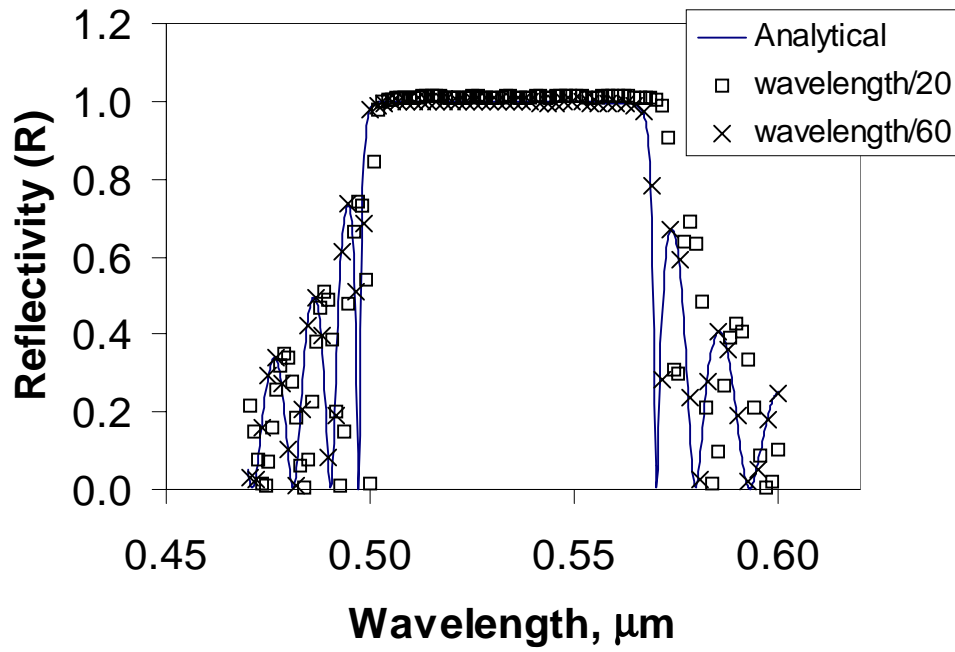


Figure 8
C. M. Titus, P. J. Bos, J. R. Kelly, E. C. Gartland
Breadth: One column, 8.5 cm.

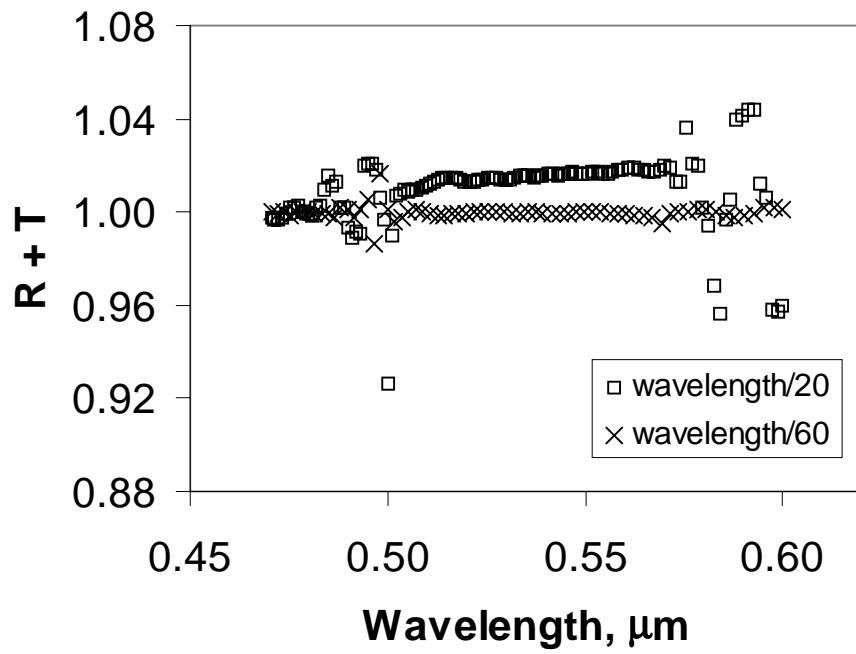


Figure 9
C. M. Titus, P. J. Bos, J. R. Kelly, E. C. Gartland
Breadth: One column, 8.5 cm.